

Large synthesis of in situ field measurements of the size distribution of mineral dust aerosols across their lifecycle

Paola Formenti¹ and Claudia Di Biagio¹

¹ Université Paris Cité and Université Paris Est Creteil, CNRS, LISA, F-75013 Paris, France

Corresponding author : Paola Formenti (paola.formenti@lisa.ipsl.fr) and Claudia Di Biagio (claudia.dibiagio@lisa.ipsl.fr)

Abstract

Mineral dust aerosol is an important contributor to the Earth climate system and the correct representation of its size distribution is fundamental for shaping the current state and the evolution of climate. Despite many observational dust size data that are available in the literature, using this body of information to properly guide the development and validation of climate models and remote sensing retrievals remains challenging. This is due to the diverse nature of different data, both in terms of measurement methods, diameter definitions, sampled concentrations and data treatments, leading to inherent heterogeneities. In this study we collect, evaluate, harmonize, and synthesize 58 size distribution data from the past 50 years of in situ field observations with the aim of providing a consistent dataset to the community to use for constraining the representation of dust size across its lifecycle. Four levels (LEV) of data treatment are defined, going from original data (LEV0), data interpolated and normalized on a standardized diameter gridpath (LEV1), and data in which original particle diameters are converted into a common geometrical definition under both spherical (LEV2a) and aspherical (LEV2b) assumptions. Size distributions are classified to be representative of as emission/source (SOURCE, <1 day from emission; number of datasets in this category, N=12), mid-range transport (MRT, 1-4 days of transport; N=36) and long-range transport (LRT, >4 days of transport; N=10). The harmonized dataset shows consistent features in the shape of the dust size distribution suggesting the conservation of airborne particles with time and a decrease of the main coarse mode diameter from located at a value of the order of 10 μm (in volume) is observed for SOURCE dust, decreasing to a value of the order of ~5 μm and ~2 μm for MRT and for LRT conditions, respectively. A for which an additional mode becomes evident below 0.4 μm for MRT and LRT dust. Data for the three levels (LEV1, LEV2a, LEV2b) and the three categories (SOURCE, MRT, LRT), together with statistical metrics (mean, median, 25% and 75% percentiles, and standard deviation) are made available as:

SOURCE (<https://doi.org/10.57932/58dbe908-9394-4504-9099-74a3e77140e9>; Formenti and Di Biagio, 2023a);

MRT (<https://doi.org/10.57932/31f2adf7-74fb-48e8-a3ef-059f663c47f1>; Formenti and Di Biagio, 2023b);

LRT (<https://doi.org/10.57932/17dc781c-3e9d-4908-85b5-5c99e68e8f79>; Formenti and Di Biagio, 2023c).

Introduction

Airborne mineral dust aerosols emitted by the aeolian erosion of bare soils contribute in a major way to the Earth's radiative budget and environmental processes, including the human health. Because of their native mineralogical composition and size distribution, they scatter, absorb, and emit interact with solar and infrared radiation, influence the formation and brightness of liquid and ice clouds, and affect the composition of the atmosphere and the ocean, while also transporting pollutants, viruses and bacteria across the continents and the oceans (Knippertz and Stuut, 2014, and the many references therein).

As a consequence, a large effort has started in the last decades to include the representation of those properties in climate and air quality models. Indeed, the complex mineralogy of mineral dust, depending

Mis en forme

Mis en forme : Soulignement , Couleur de police : Bleu

Mis en forme

45 on that of the parent soils (Claquin et al., 1999; Journet et al., 2014; Gonçalves Ageitos et al., 2023a), is
46 now accounted for in models (Scanza et al., 2015; Perlwitz et al., 2015a; 2015b; Menut et al., 2020; Kok
47 et al., 2017; Di Biagio et al., 2020; Gómez Maqueo Anaya et al., 2024³) and starts to be retrieved by
48 remote sensing (Green et al., 2020; Zhou et al., 2020; Di Biagio et al., 2023).

49 On the other hand, representing the span and the variability in time and space of the dust aerosol size
50 distribution remains a challenge.

51 The particle size distribution of mineral dust extends over several orders of magnitudes. Iron-rich
52 particles as small as 14 nm in diameter have been observed in the laboratory from deflating soils by
53 Baddock et al. (2013). During sandstorm in Algeria, Gomes et al. (1990) measured an increase of the
54 mass concentration of particles between 100 nm and 1 μm , and attributed [this](#) to clays disaggregated
55 by sandblasting. Measurements of the size-resolved vertical dust flux by Gillette et al. (1972; 1974a;
56 1974b) based on microscopy analyses of samples from Texas and Nebraska showed the presence of
57 particles up to several microns in dust emissions.

58 The representation of the accumulation and coarse modes in mineral dust has long been based on the
59 columnar measurements by the sun/sky photometers of the Aerosol Robotic Network (AERONET)
60 network, which provides with normalized size distributions of mineral dust considered as chemically
61 homogeneous particles the 0.1–30 μm optically-equivalent diameter (Dubovik et al., 2002; 2006;
62 Holben et al., 2011), and which, incidentally, serve also the look-up tables of the remote sensing
63 retrievals of dust from space (e.g., Cuesta et al., 2015; Zhou et al., 2020).

64 Nevertheless, in situ observations at ground-based stations and on aircraft in more recent years have
65 shown that particles of several tens, sometimes hundreds, of micron are airborne at emission, and
66 remain so after several days of transport (Reid et al., 2003; Formenti et al., 2003; Rajot et al., 2008;
67 Chou et al., 2008; Kandler et al., 2007; 2009; Wagner et al., 2009; Klaver et al., 2011; Ryder et al., 2013;
68 2015; Rosenberg et al., 2014; Denjean et al., 2016; Wienzerl et al., 2017; van der Does et al., 2018).

69 These observations have been instrumental to a number of advances. Using them as ensemble dataset,
70 to smooth ~~spurious-local~~ atmospheric variability, they have served as a basis to a new classification of
71 the dust size distribution in four modes, namely fine dust (diameter $\leq 2.5 \mu\text{m}$), coarse dust ($2.5 <$
72 $\text{diameter} \leq 10 \mu\text{m}$), super coarse dust ($10 < \text{diameter} \leq 62.5 \mu\text{m}$) and giant dust (diameter $> 62.5 \mu\text{m}$),
73 extending above the size range retrieved by AERONET (Adeyemi et al., 2023). Additionally, they have
74 also fostered the revision of the numerical schemes of emissions and deposition, and identified the
75 numerous processes and properties (non-spherical shape of particles, electric forces, atmospheric
76 turbulence), that could counteract the size-selective removal by gravitational settling and keep particles
77 airborne longer than expected (Kok, 2011; Huneeus et al., 2011; Mahowald et al., 2011; Kok et al., 2017;
78 Di Biagio et al., 2020; Zhao et al., 2022; Adebisi and Kok, 2020; Adebisi et al., 2020; Huang et al., 2021;
79 Meng et al., 2022; Adeyemi et al., 2023).

80 In support of those activities, in this paper we present a large and standardized compilation of *in situ*
81 observations of the particle size distribution of mineral dust conducted during the past 50 years of
82 research. This dataset extends the currently published [ensembles compilations of measurements](#) (Meng
83 et al., 2022; Adeyemi et al., 2020; 2023) to provide with a state-of-the-art of the current knowledge in
84 support to the development of models, and ground-based and satellite remote sensing. Analysis of this
85 dataset may provide with an integrated view of the size distribution of dust particles across their life
86 cycle to evaluate their impacts in the Earth/human system.

87 2. Methods

88 2.1 Constitution of the dataset

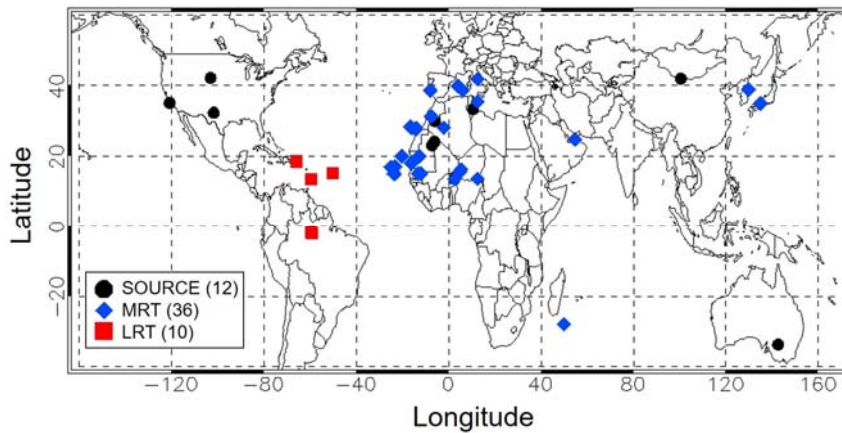
Mis en forme

89 Data presented in this paper result from in situ ground-based and aircraft observations of airborne dust
90 conducted during field campaigns during the past 50 years of dust research. Data from deposition
91 samples (e.g., van der Does et al. 2018 or Varga 2021) are not considered in this analysis.

92 Only datasets being published and properly referenced in the open peer-reviewed literature were
93 retained. We also privileged datasets for which the methodology of acquisition, calibration and data
94 treatment was well described so that the data quality can be assessed. Finally, we search for data as
95 much as possible representative of different source and transport regions of the world.

96 The observations contributing to the dataset are listed in **Table S1** and the spelling of the acronyms of
97 the field campaigns is reported in **Text S1** in the supporting material. Data are geo-localized in **Figure 1**,
98 where they are classified with respect to their time after emission. [Geographical coordinates are](#)
99 [reported in Table S2.](#)

100
101
102



103
104

105 **Figure 1.** Geographical location of the datasets contributing to size distribution observations for the source, the
106 mid-range transport (MRT) and the long-range transport (LRT) categories. The legend indicates the line style
107 used in the plot. The number of data for each category is indicated in the parenthesis in the legend.

108

109 Observations obtained at the time of dust emission or within 1 day after emission are classified as
110 SOURCE. Observations corresponding to 1 to 4 days after emission and/or geographically acquired
111 near-source regions (for example, offshore North Africa) are classified as mid-range transport (MRT).
112 Observations at times exceeding 4 days after emission or geographically distant from source regions
113 (for example, observations in the Caribbean) are classified as long-range transport (LRT). [To note that](#)
114 [potential uncertainties may arise in this classification, in particular for datasets lying at the boundaries](#)
115 [of the SOURCE, MRT and LRT categories, and we acknowledge this aspect as a source of error in our](#)
116 [analysis. We invite the reader to refer to the Supplementary material \(Text S4\) for thorough description](#)
117 [of the assumptions made in some cases to associate each dataset to a category.](#)

118 The SOURCE dataset (Fig 1, black points) consists in 12 observations in Northern Africa, North America,
119 and Asia, and one data point set in Australia. They include works by Gillette et al. (1972, 1974), Gillette
120 (1974), Fratini et al. (2007), Rajot et al. (2008), Sow et al. (2009), Shao et al. (2011), Ryder et al. (2013a,
121 2013b), Rosenberg et al. (2014), Huang et al. (2019), and Khalfallah et al. (2020), a set of data recently
122 used by Kok et al. (2017), Di Biagio et al. (2020) and Huang et al. (2021) to constrain the shape of dust
123 size distribution at emission in model studies, and the most recent work by Gonzales-Florez et al. (2023).

Mis en forme

124 The MRT class (Fig. 1, blue points) is contributed by 36 datasets from field campaigns (ACE2, ACE-Asia,
125 ADRIMED, AER-D, AMMA, DABEX, DARPO, DIAPASON, DODO1-2, FENNEC, GAMARF, GERBILS, INDOEX,
126 NAMMA, RHaMBLe, SALTRACE, SAMUM1-2, TRACE-P, and UAE2) in Western Africa, Capo Verde, the
127 Mediterranean basin, the eastern tropical Atlantic, Saudi Arabia, Japan, and Indian Ocean, downwind
128 sources either over the ocean or over desert areas. Additional datasets from studies performed in the
129 Sahara, the Atlantic Ocean, Canary Islands and Japan (SchutzSchütz, 1981; D’Almeida et al., 1987;
130 Maring et al., 2000; Kobayashi et al., 2007) are added to the dataset. The LRT class (Fig. 1, red points)
131 lays on 10 datasets of observations across the Atlantic Ocean and South America and is contributed by
132 observations from Bacex, CLAIRE, Dust-Attack, Go-Amazon, PRIDE, and SALTRACE campaigns and
133 intercontinental dust transport data from Schutz-Schütz (1981).

134 2.2. Instrumentation contributing to the in situ dataset

135 The natural dynamical range of the particle size and concentration of mineral dust can only be
136 represented by a combination of instruments based on different intrinsic particle properties such as
137 density, electrical charge, shape and composition (e.g., Reid et al., 2003a; Formenti et al., 2011;
138 Wendisch and Brenguier, 2013; Mahowald et al., 2014, Adeyemi et al., 2023). As a consequence, the
139 datasets considered in this paper are contributed by different in situ instruments, also described in **Text**
140 **S2** in the supporting material, namely:

- 141 o Optical particle counters (OPC) using the dependence of light scattering on particle size and providing
142 with the particle concentration as a function of the optical equivalent diameter (e.g., Reid et al.,
143 2003b; Clarke et al., 2004; Osborne et al., 2008; Formenti et al., 2011; Ryder et al., 2013a, 2018;
144 Khalfallah et al., 2020).
- 145 o Particle collection by filtration or impaction followed by individual particle characterization by
146 transmission (TEM) and/or scanning electron microscopy (SEM) sizing particles as function of their
147 equivalent projected-area diameter and coulter geometric sizing methods, (e.g., Gillette et al., 1972,
148 1974a, 1974b; Reid et al., 2003a; Khobayashi et al., 2007; Kandler et al., 2009; Chou et al., 2008).
- 149 o Multi-stage filtration or impaction sampling coupled with gravimetric or chemical analysis providing
150 with the mass size distribution as equivalent aerodynamic diameter (e.g., Formenti et al., 2001; Reid
151 et al., 2003b).
- 152 o Differential and Scanning Mobility Particle Sizer (DMPS and SMPS) providing the size of particles in
153 the submicron range as the electrical mobility equivalent diameter of a charged particle moving in a
154 static electric field (e.g., Maring et al., 2000, 2003; Bates et al., 2002; Muller-Müller et al., 2010;
155 Denjean et al., 2016a, 2016b).
- 156 o Aerodynamic particle sizers (APS), measuring the equivalent aerodynamic diameter of a sphere of
157 unit density having the same terminal velocity in an accelerated airflow as the irregularly shaped
158 dust particles (e.g., Maring et al., 2003; Reid et al., 2003b; 2008; Struckmeier et al., 2016)

159 Each of those instrument types sizes particles on an equivalent diameter (optical, projected-area,
160 aerodynamic, mobility) that depends on their respective working principle. Converting those
161 operational size definitions into a homogenized one is part of the treatment applied in this work, which
162 follows the theory proposed and discussed in the literature and benefits of recent progresses in
163 characterizing/synthesizing dust properties relevant for these treatments (e.g., Hinds, 1999, De Carlo et
164 al., 2004 ; Mahowald et al., 2014; Di Biagio et al., 2019; Huang et al., 2020, 2021; Formenti et al., 2021).
165 Diameter definitions and formulas to convert each of them into a geometrical diameter, both under the
166 assumption of spherical and aspherical dust, is provided in **Text S3** and summarized in **Table S2S3**.

167 **Text S4** presents relevant information on each dataset considered in the present analysis. This includes
168 a brief description of the field operations, the experimental conditions, the type of original data
169 (number, volume or mass concentration size distribution, size-resolved emission fluxes), the
170 instrumentation, and the data treatment applied to the measurements (averages, diameter corrections,

Mis en forme

171 etc.) in the original publication. Original data were obtained, as much as possible, through a personal
172 contact with the data providers or from the original publications ~~based on a digitalization procedure~~
173 ~~using online tools (<https://automeris.io/WebPlotDigitizer/>)~~. This is also indicated in **Text S4**.

174 **2.3. Data treatment, harmonization, and synthesis**

175 The original observations were treated to provide with a harmonized dataset ~~both~~ in terms of the
176 definition of particle diameter ~~and data were and normalized to remove~~ differences in sampled number
177 concentrations. Four level of data treatment are defined as described below.

178 1/ *Level-0 (LEVO)*: original data, taken at the native resolution or the resolution from digitalization
179 process and converted into volume distribution assuming spherical particles ($\pi/6 * D^3 * dN/d\log D$), where
180 D is the particle diameter used in the publication and $dN/d\log D$ is the particle number concentration.
181 ~~For starting to removing~~ differences ~~due to sampling in~~ concentration, and in absence of information
182 on original bin width ~~in the majority of cases~~, *LEVO* data are normalized ~~so that to~~ the maximum of the
183 volume size distribution ~~is equal to 1~~;

184 2/ *Level-1 (LEV1)*: data from *LEVO* are interpolated over a common size range of equi-logarithmically
185 spaced diameters ($d\log D = 0.05$) encompassing the original diameter range for each dataset and
186 normalized so that the integral is equal to 1 over a common diameter range. The diameter range for
187 integral normalization was set to be the largest as possible and to be covered by more than 90% of the
188 datasets in each category. For SOURCE data it resulted that the diameter range for common integral
189 normalization is within 1.58 and 7.1 μm , and for MRT and LRT it is between 0.71 and 8.9 μm .

190 3/ *Level-2a (LEV2a)*: based on *LEV1*, the *LEV2a* data treatment aims at harmonizing the size distributions
191 by converting the operational original particle diameters, which depend on the physical principle of each
192 instrument, into a common-defined sphere-equivalent geometric diameter. Data from *LEV1* are
193 treated as in the following with respect to their diameter corrections:

- 194 ○ data already provided as geometrical diameters (from coulter counters, i.e., ~~only one only~~
195 dataset in our study) are left unchanged;
- 196 ○ data provided as projected-area diameters (i.e. from microscopy) are left unchanged;
- 197 ○ data provided as aerodynamic diameters (from APS or cascade impactors) are corrected
198 assuming a shape factor (χ) of 1 (under spherical assumption), therefore a size-invariant
199 conversion factor of 1.58 (see Eq. S2) is applied to the dataset assuming dust density of 2.5 g
200 cm^{-3} ($D_{\text{geom}} = D_{\text{aerod}}/1.58$). If original aerodynamic diameter data are already converted into
201 geometrical diameter, we replace the original correction with the conversion factor of 1.58.
202 Since the correction is a multiplicative factor the $d\log D$ of the bins remain unchanged;
- 203 ○ data provided as optical diameters (from OPCs) are converted into sphere-equivalent
204 geometric diameters applying the optical to geometrical correction by assuming homogeneous
205 spherical particles and a value of CRI of 1.53–0.003i. ~~This CRI value is at the average of the dust~~
206 ~~refractive indices reported in the 370-950 nm spectral range in Di Biagio et al. 2019) for dust of~~
207 ~~global origin~~. Data for applying the correction for the different model of OPCs considered were
208 taken from Formenti et al. (2021) and conversion factors were recalculated at the $d\log D$ path
209 of 0.05 assumed in the interpolated sizes. For the GRIMM 1.108 for which calibration is not
210 provided in Formenti et al. (2021) we used the data taken from Formenti et al. (2011) (~~For-~~
211 ~~menti, personal communication~~) interpolated at the 0.05 $d\log D$ path of our diameters. In
212 order to avoid discontinuities appearing and because of the new $d\log D$ do not significantly differ
213 on average from the value of 0.05 for D_{geom} calculated from D_{opt} interpolated data, we do not
214 update the $d\log D$, so that the conversion only imply a shift of the diameter. More details on the
215 choices applied for corrections in different cases are provided in Text S4. Original datasets
216 already converted into geometrical diameter, are left unchanged. However, it is worth ~~to~~
217 ~~noting~~ that the ensemble of data already applying an optical to geometrical correction uses
218 a CRI varying between 1.53 and 1.55 for the real part and 0.001 and 0.004 for the imaginary

Mis en forme

219 part and work under the hypothesis of homogeneous spherical particles (Mie theory), therefore
220 consistent with our treatment. Exceptions are Khalfallah et al. (2020) using a CRI of 1.43–0.00i
221 as for quartz particles, and González–Flórez et al. (2023) using a CRI of 1.49–0.0015i and also
222 applying calculations in ellipsoidal assumption instead of Mie theory. The only dataset not
223 theoretically submitted to the optical to geometric correction is the one provided by Renard et
224 al. (2018) using an OPC built with a specific geometry making the measurements very low
225 sensitive to CRI calibration.

226 *4/ Level–2b (LEV2b)*: based on LEV1, the LEV2b data treatment aims at harmonizing the size distributions
227 by converting the operational original particle diameters into a common–defined geometrical diameter
228 by taking into account that mineral dust is aspherical. Data from LEV1 are treated as in the following
229 with respect to their diameter corrections:

- 230 ○ data already provided as geometrical diameters from coulter counters are left unchanged. This
231 technique is in fact only slightly affected by shape effects, as discussed by Kobayashi et al.
232 (2007);
- 233 ○ data provided as projected–area diameters are corrected using the size–invariant correction
234 factor of 1.56 from Huang et al. (2021) ($D_{\text{geom}}=D_{\text{area}}/1.56$) (see Eq. S1);
- 235 ○ data provided as aerodynamic diameter are corrected assuming a size–invariant conversion
236 factor of 1.45 following Huang et al. (2021) ($D_{\text{geom}}=D_{\text{aerod}}/1.45$) (see Eq. S2);
- 237 ○ data provided as optical diameters and already treated as for LEV2a data, are further corrected
238 by applying a size–dependent aspherical to spherical ratio ($\text{ASR}(D_{\text{geom}})$) correction function,
239 $\text{ASR}(D_{\text{geom}})=(D_{\text{geom}})_{\text{aspherical}}/(D_{\text{geom}})_{\text{spherical}}$, to take into account non–sphericity effects in optical to
240 geometrical conversion. The ASR function (Fig. S1) is obtained by combining the optical to
241 geometrical diameter conversion factors for different OPCs calculated by Formenti et al. (2021)
242 and Huang et al. (2021) both in the assumption of spherical homogeneous particles ($(D_{\text{geom}})_{\text{spherical}}$
243 and tri–ellipsoids dust ($(D_{\text{geom}})_{\text{aspherical}}$). More details are provided in Text S3. Original datasets
244 derived from OPC measurements already provided as geometrical diameter but under
245 assumption of sphericity are also corrected by applying the $\text{ASR}(D_{\text{geom}})$ converting function. The
246 only exception are González–Flórez et al. (2023), that already apply tri–axial ellipsoids
247 calculations in their optical to geometric conversion, and Renard et al. (2018), not requiring
248 optical to geometrical conversion.

249 As for LEV1, the LEV2a and LEV2b data, for which a known interpolation path is used, are normalized so
250 that the integral of the volume size distribution is 1 over a common diameter range (1.58 – 7.1 μm for
251 SOURCE, 0.71 – 8.9 μm for MRT, LRT).

252 For each category (SOURCE, MRT, LRT) and for each data level (LEV1, LEV2a, LEV2b), the mean, median,
253 and standard deviation of the particle volume concentration per size class are calculated where at least
254 2 datasets are available in the diameter range. Additionally, the 25% and 75% percentiles are also
255 calculated, despite keeping in mind their limited representativeness given the reduced number of
256 samples in the datasets, especially for SOURCE and LRT classes.

257 ▲ ----- 258 **2.4. Limitations of the ~~proposed-chosen~~ approach**

259 Some precisions should be given when considering the LEV2a and LEV2b treatment reported in this
260 work. First, the implicit assumption when applying LEV2a and LEV2b dataset corrections is that dust is
261 the dominant aerosol species and possible effects due to internal or external mixing of dust with other
262 aerosol types are not taken into considerations (i.e., in the complex refractive index or shape factor
263 assumptions). Second, for those datasets that are obtained from the combination of different
264 techniques, namely DMPS+APS (Bates et al., 2002; Maring et al., 2000, 2003; Müller–Müller et al., 2010),
265 OPC+APS (Chen et al., 2011), SMPS + OPC (de Reus et al., 2000; Otto et al., 2007; Denjean et al., 2016a,
266 2016b), DMPS + APS + microscopy (Kandler et al., 2011), or multiple OPC instruments (Reid et al., 2003b;

Mis en forme : Anglais (Royaume-Uni)

Mis en forme

267 McConnell et al., 2008; Johnson and Osborne, 2011; Ryder et al., 2013a, 2013b, 2018; Rosenberg et al.,
268 2014; Weinzierl et al., 2009, 2011, 2017), the choice is that of applying artefact corrections for the
269 dominant instrument, often the one in the extended coarse mode range, and consider this correction
270 applicable to the whole diameter range. This is because when multiples instruments are used to build a
271 size distribution it is then not easy to reconstruct the steps of data analysis and merging from the original
272 work. It follows the subsequent considerations:

273 1/ the corrections applied for the aerodynamic and projected-area diameter apply a constant
274 size-invariant scaling factor to the ensemble of the size distribution data. In this approximation, if
275 the SMPS/DMPS is combined with aerodynamic or microscopy data, a correction factor between
276 1.45 and 1.58, depending on the level and the technique as detailed in the previous section, is
277 applied in place of the factor 1 (spherical assumption) or 1.19 (aspherical assumption) (see Eq. S3)
278 expected to convert the mobility diameter to geometrical diameter in LEV2a and LEV2b data. As a
279 consequence, the submicron size is 20 to 58% finer than expected only due to mobility to geometrical
280 conversion.

281 2/ A similar approach is used to correct datasets where OPC is the main used technique to size dust
282 particles together with the SMPS. For LEV2a data the Mie correction is applied to the full size
283 distribution, but being the size-dependent correction mostly inactive for submicron particles (i.e.
284 $D_{\text{geom}} \sim D_{\text{opt}}$ for most OPCs), the approach is mostly equivalent at considering a mobility diameter
285 correction with a shape factor of 1. For LEV2b data, using OPC corrections induce a limited right
286 shifting of the size distribution compared to the one that would be obtained from mobility
287 conversion because of the magnitude of the ASR function (Fig. S1) compared to the shape factor of
288 1.19 assumed for aspherical dust.

289 3/ When datasets relying on multiple OPCs measurements, the assumption is that the “dominant” OPC
290 that is the OPC covering the largest range and the coarsest sizes in particular, is considered. Given
291 that optical to geometrical corrections are not relevant for submicron particles and that the
292 magnitude of the correction typically increases for increasing sizes, this assumption is not expected
293 to determine significant biases in the data. To mention additionally a general ambiguity of the optical
294 to geometrical correction around the diameter of 1 μm where a plateau in the scattering calibration
295 function for several OPCs models can be found (i.e. Formenti et al., 2021).

296 More details on the specific assumptions and choices done for each dataset are provided in **Text S4**.

297 Further, for LEV2a and LEV2b data for which corrections are applied on the data, caution is taken at the
298 boundary of the size distribution and when the first and/or the last bin of the corrected size showed
299 unrealistic significant divergence, these data are removed from the dataset.

300 To note that an additional source of error, not possible to estimate robustly because of the lack of
301 detailed information for all datasets, is the individual measurement uncertainty, which varies with the
302 specific setup, instrument and spatial and temporal extent of the measurement.

303

304 3. Presentation and discussion of the dataset

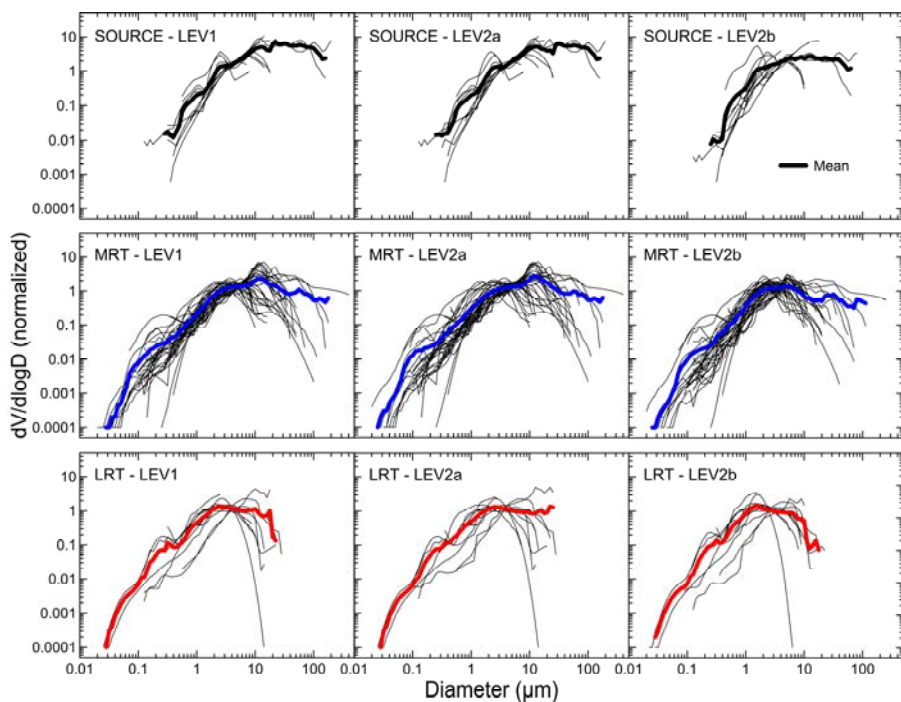
305 Illustration of the data for different levels is provided in Figure 2. Figure 3 presents the synthesis of the
306 LEV2b data and the comparison of SOURCE, MRT and LRT distributions. The contribution of different
307 size classes to the total particle number, surface and volume is summarised in Table 1. Size classes have
308 been defined according to the classification of Adeyemi et al. (2023) defining fine dust ($D \leq 2.5 \mu\text{m}$),
309 coarse dust ($2.5 < D \leq 10 \mu\text{m}$), super coarse dust ($10 < D \leq 62.5 \mu\text{m}$) and giant dust ($D > 62.5 \mu\text{m}$). Within
310 the fine dust class, we further calculate the fractions of particles smaller than 0.4 μm .

311

Mis en forme : Anglais (Royaume-Uni)

Mis en forme

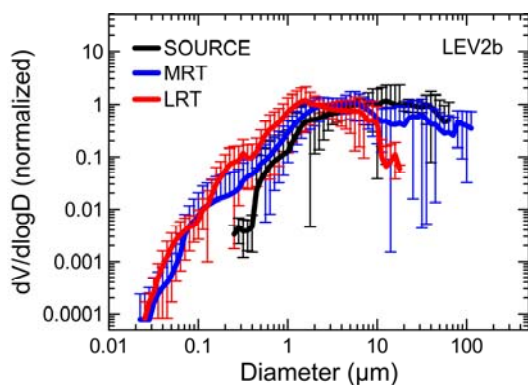
312



313

314 **Figure 2.** Data for SOURCE, MRT, and LRT dust at level 1, 2a, and 2b as described in Sect. 2.3 (labelled as LEV1,
315 LEV2a, LEV2b, respectively). Single datasets, all normalized at the integral of 1, are plotted as black lines. The mean
316 (thick black, blue, and red line for SOURCE, MRT, and LRT, respectively) are shown at all levels. Note that the mean
317 is calculated only where at least 2 datasets are available in the diameter range.

318



319

320 **Figure 3.** Comparison of normalized mean volume size distribution for the SOURCE, MRT, and LRT categories in our study
321 reported as LEV2b data (mean \pm standard deviation). For the sake of comparison, and differently from data in Fig. 2, the
322 SOURCE, MRT, and LRT synthesis datasets reported here are normalized at the integral equal to 1 over a common diameter
323 range corresponding to 0.35–17.8 μm . This is done to remove differences linked to different integration range for SOURCE data
324 compared to MRT and LRT.

Mis en forme : Justifié

Mis en forme : Justifié

Mis en forme

325
326

Dataset		$D \leq 2.5 \mu\text{m}$ ($D \leq 0.4 \mu\text{m}$)	$2.5 < D \leq 10 \mu\text{m}$	$10 < D \leq 62.5 \mu\text{m}$	$D > 62.5 \mu\text{m}$
Number	SOURCE	95.4% (20.4%)	4.5%	0.1%	0.4%
	MRT	99.8% (96.1%)	0.2%	0.0%	0.0%
	LRT	99.9% (94.5%)	0.1%	0.0%	0.0%
Surface	SOURCE	45.0% (1.1%)	39.4%	15.5%	0.14%
	MRT	65.4% (16.8%)	30.7%	3.6%	0.29%
	LRT	84.6% (23.1%)	15.1%	0.2%	0.00%
Volume	SOURCE	10.8% (0.1%)	34.9%	52.7%	1.6%
	MRT	22.1% (1.1%)	44.3%	25.7%	8.0%
	LRT	53.4% (3.6%)	44.5%	2.0%	0.0%

Tableau mis en forme

327 **Table 1.** Percentages of number, surface and volume size distribution in the diameter ranges $D \leq 0.4 \mu\text{m}$, $D \leq 2.5 \mu\text{m}$, $2.5 < D \leq$
328 $10 \mu\text{m}$, $10 < D \leq 62.5 \mu\text{m}$, and $D > 62.5 \mu\text{m}$ for the mean of the size obtained for the SOURCE, MRT, and LRT LEV2b datasets.

329

330 As shown in Fig. 2 and 3 the shape of the dust size distribution at emission and along transport shows
331 main consistent features. A main mode located at $\sim 10 \mu\text{m}$ (in volume) is observed for dust at emission
332 and close to sources, [as based from the few studies allowing to measure up to the coarse fraction](#). The
333 main dust mode decreases to $\sim 5 \mu\text{m}$ and $\sim 2 \mu\text{m}$ for MRT and LRT conditions, respectively. Below $0.4 \mu\text{m}$
334 the dust volume size shows an additional mode, particularly visible for MRT and LRT. As a matter of fact,
335 the sparse datasets measuring very fine particles at the SOURCE show that particles with diameters
336 below $0.4 \mu\text{m}$ (however measured only down to $0.2 \mu\text{m}$, as shown in Fig. 2) represent approximately
337 20% of the total particles' number, increasing to more than 90% in MRT and LRT. Instruments such as
338 SMPS and DMPS used in MRT and LRT studies measure particles as small as $0.02 \mu\text{m}$ in diameter.
339 Previous single-particle compositional observations showing that the particle number concentration in
340 the size range between 0.1 and $0.4 \mu\text{m}$ is largely contributed by aluminosilicate dust particles at
341 emission, while internal or external mixing with aerosols other than dust gains importance with time
342 and altitude of transport (Chou et al., 2008; Kandler et al., 2007, 2009; Weinzierl et al., 2009; 2017;
343 Klaver et al., 2011; Denjean et al., 2016a; 2016b).

344 The [normalized](#) size distribution of dust particles between 0.4 and $10 \mu\text{m}$ is rather consistent and
345 invariant along the dust cycle. This is true in particular when restricting to the 2.5 to $10 \mu\text{m}$ size range
346 when differences are minimal and contribution to total volume is in between 34.9% and 44.5% . Below
347 that range, which is between 0.4 and $2.5 \mu\text{m}$, the contribution of particles for LRT is significantly higher
348 (53.4% in volume) than for SOURCE (10.8%) and MRT (22.1%), likely as, because of the normalization, it
349 compensates the decrease of particles larger than $10 \mu\text{m}$.

350 The [intensity-magnitude](#) of the particle volume above $10 \mu\text{m}$ remains unchanged almost up to $100 \mu\text{m}$
351 for both the SOURCE and the MRT conditions, which also present similar particle volume. This mode
352 decreases very strongly for LRT conditions, when it represents only 2% of the total volume, compared
353 to almost 55% and 34% for SOURCE and MRT, respectively.

354 The dataset presented in this work, synthetizing available *in situ* observations, allows ~~to~~
355 [evaluate](#) ~~evaluation of~~ the natural variability of dust size distribution along its lifecycle. To be
356 emphasized, however, that while consistent differences in the mean size distribution curves are
357 obtained going from SOURCE to LRT, as shown in Fig. 3, the inherent range of variability for each
358 category, represented by the standard deviation of the data, is also non-negligible and reflects the large
359 range of documented size distributions, together with the limited statistics available. This is particularly
360 true for both super-coarse and giant dust at MRT and LRT. Lower variability is identified below $0.4 \mu\text{m}$
361 ~~, but~~ because of the restricted number of dataset available for MRT and LRT conditions, ~~while we~~
362 [identify](#) ~~and there is~~ an absence of data for SOURCE dust below this size range.

Mis en forme

363 Finally, to facilitate the use of these data within help making results from models and remote sensing
 364 studiechemes on mineral dust more comparable, Table 2 provides multi-modal the parameters of
 365 lognormal size distributions fitting the LEV2a and LevEV2b mean values of the three dust
 366 categories. Lognormal functions are set
 367 to reproduce the main shape of the dust distribution above 0.4 μm , neglecting the specific features
 368 below this diameter where information is lower and the size affected by particle mixing with other
 369 compounds, especially for MRT and LRT. We found that a single broad mode ~~three to five modes~~ can be
 370 employed ~~are necessary~~ to represent the major features of the volume-number size distributions
 371 above 0.4 μm and their variability with size. Only LRT2a data can be also fitted with a single mode
 372 (geometric median diameter 2 μm and geometric standard deviation 2.7). Plots of the fitting functions
 373 are provided in supplementary Fig. S4. Because there is an inherent level of subjectivity in the choice of
 374 the number of modes and their parameters, we invite the individual researchers using the data to
 375 implement the parameterizations in accordance to their scientific needs.

Dataset	Lognormal mode				
	N_{tot} ($\# \text{ cm}^{-3}$)	NMD (μm)	V_{tot} ($\text{nm}^3 \text{ cm}^{-3}$)	VMD (μm)	σ
SOURCE – LEV2a	$5.08 \cdot 10^{-10}$	0.355	7.76	26.69	3.32
SOURCE – LEV 2b	$9.8 \cdot 10^{-10}$	0.300	3.38	11.71	3.02
MRT – LEV 2a	$2.11 \cdot 10^{-9}$	0.150	2.55	11.64	3.33
MRT – LEV 2b	$6.82 \cdot 10^{-9}$	0.100	1.57	5.79	3.20
LRT – LEV 2a	$2.35 \cdot 10^{-9}$	0.280	1.39	3.88	2.55
LRT – LEV 2b	$2.96 \cdot 10^{-9}$	0.350	1.15	2.34	2.22

Mis en forme : Police :Non Gras

Tableau mis en forme

378
 379
 380 **Table.** Parameters (total number and volume concentration, N_{tot} ($\# \text{ cm}^{-3}$), V_{tot} ($\text{nm}^3 \text{ cm}^{-3}$), number and volume median diameter,
 381 NMD and VMD (μm), geometric standard deviation, σ) for the log-normal modes used to parameterize the LEV2b volume size
 382 distributions of the SOURCE, MRT, and LRT categories. Parameters refers to the following equations: $\frac{dv}{d\log D} =$
 383 $\frac{\pi}{6} D^3 \frac{N_{tot}}{\sqrt{2\pi} \log \sigma} \exp\left(-\frac{(\log D - \log NMD)^2}{2(\log \sigma)^2}\right)$ and $\frac{dv}{d\log D} = \frac{V_{tot}}{\sqrt{2\pi} \log \sigma} \exp\left(-\frac{(\log D - \log VMD)^2}{2(\log \sigma)^2}\right)$

Mis en forme : Justifié

384 385 4. Conclusive remark

386 In this paper we present the most possible comprehensive synthesis of *in situ* observations of the
 387 particle size distribution of atmospheric dust aerosols. This compilation reflects the current state-of-
 388 the-art and represents a standardized and synthetic benchmark to constrain and evaluate models and
 389 satellite retrievals. We highlight differences and commonalities of the dust volume distribution as a
 390 function of time in the atmosphere, both in terms of main identified modes and relative contribution of
 391 dust in different size ranges.

392 We did this based on Aa large statistics of data is available and permit to retrieve robust information
 393 between 0.4 and 10 μm where most of observations exist, while above and below this size range,
 394 observations are rare. Dust particles below 0.4 μm in diameter are seldom measured close to source
 395 regions, but are found in observations at mid- and long-range transport conditions. Their presence at
 396 emission, their size-segregated composition and state of mixing should be better documented and
 397 understood. The dynamics of the coarse mode above 10 μm , its invariance from source to mid-range
 398 transport, and decline afterwards is reported, and can challenge models.

399 We acknowledge the evidence that the compilation of a reference dataset is, almost by definition, a
 400 subjective and incomplete exercise which must revised continuously with the emergence of new

Mis en forme

401 datasets, new field campaigns, and the improvement of sampling techniques. We henceforth encourage
402 colleagues to provide us with new or revised datasets to feed and update the dataset in the future.

403 Data availability

404 The LEV1, LEV2a and LEV2b datasets discussed in this paper are available on the EaSy Data, the Earth
405 System Data repository (<https://www.easydata.earth/#/public/home>, last access: ~~0114 June~~
406 ~~2023~~2024) maintained by the National French DATA TERRA research Infrastructure. Their respective
407 DOIs are summarized here below:

408 SOURCE_LEV1.dat, SOURCE_LEV2a.dat, SOURCE_LEV2b.dat : <https://doi.org/10.57932/58dbe908-9394-4504-9099-74a3e77140e9> (Formenti and Di Biagio, 2023a);

410 MRT_LEV1.dat, MRT_LEV2a.dat, MRT_LEV2b.dat: <https://doi.org/10.57932/31f2adf7-74fb-48e8-a3ef-059f663c47f1> (Formenti and Di Biagio, 2023b);

412 LRT_LEV1.dat, LRT_LEV2a.dat, LRT_LEV2b.dat : <https://doi.org/10.57932/17dc781c-3e9d-4908-85b5-5c99e68e8f79> (Formenti and Di Biagio, 2023c).

414 Figures of the individual datasets (including LEV0) are provided upon request.

415 Code availability. ~~Data from images on published papers were digitalized with the online~~
416 ~~WebplotDigitizer software available at <https://automeris.io/WebPlotDigitizer/>~~

Mis en forme : Police :Gras

417 **Author contributions.** PF and CDB designed the research, compiled and analysed the dataset, ~~and~~
418 ~~analysed it,~~ and wrote the manuscript.

419 **Competing interests.** The authors declare that they have no competing interests.

420 **Special issue statement.** The paper is not associated with a special issue.

421 Acknowledgements

422 PF and CDB acknowledge J. L. Rajot, C. Denjean, A. Adeyemi, D. Meloni, C. Ryder, and J. Kok for
423 providing the original data from their publications. ~~The help of G. Brissebrat to create the DOI for the~~
424 ~~different datasets is gratefully acknowledged. The authors would like to thank G. Schuster~~
425 ~~(NASA/Langley), R. Miller (NASA/Giss) and the second anonymous referee for their effort in improving~~
426 ~~the paper and the data access. The help of G. Brissebrat (CNRS/DATA TERRA/Aeris), H. Bressan and S.~~
427 ~~Grellet (GaiaData BRGM) in creating to create the DOI for the different datasets and solving the access~~
428 ~~issues is gratefully acknowledged.~~

Mis en forme : Couleur de police : Automatique

Mis en forme : Gauche, Espace Avant : Automatique,
Après : Automatique

Mis en forme : Couleur de police : Automatique,
Anglais (Royaume-Uni)

Mis en forme : Police : (Par défaut) + Titres (Calibri
Light), Anglais (Royaume-Uni)

Mis en forme : Couleur de police : Automatique,
Anglais (Royaume-Uni)

Mis en forme : Couleur de police : Automatique,
Anglais (Royaume-Uni)

Mis en forme : Police :Non Gras, Anglais

429 Funding

430 This research is funded by the project DustClim, part of ERA4CS, an ERA-NET initiated by JPI Climate,
431 and funded by FORMAS (SE), DLR (DE), BMWFW (AT), IFD (DK), MINECO (ES), ANR (FR) with co-funding
432 by the European Union (Grant 690462).

Mis en forme

433 **References**

434 Adebisi, A. A., and Kok, J. F.: Climate models miss most of the coarse dust in the atmosphere, *Science Advances*,
435 6, eaaz9507, doi:10.1126/sciadv.aaz9507, 2020.

436 Adebisi, A. A., Kok, J. F., Wang, Y., Ito, A., Ridley, D. A., Nabat, P., and Zhao, C.: Dust Constraints from joint
437 Observational–Modelling–experimental analysis (DustCOMM): comparison with measurements and model
438 simulations, *Atmos. Chem. Phys.*, 20, 829–863, <https://doi.org/10.5194/acp-20-829-2020>, 2020.

439 Adebisi, A. A., [Jasper J. Kok](#), [Benjamin J Murray](#), [Claire L Ryder](#), [Jan Berend B. W. Stuut](#), [Ralph R. A. Kahn](#), [Peter](#)
440 [P. Knippertz](#), [Paola P. Formenti](#), [Natalie N. M Mahowald](#), [Carlos C. Pérez García-Pando](#), [Martina Klose](#), [Albert A.](#)
441 [Ansmann](#), [Bjorn-B. Hallvard H. Samset](#), [Akinori A. Ito](#), [Yves-Y. Balkanski](#), [Claudia C. Di Biagio](#), [Manolis M. N.](#)
442 [Romanias](#), [Yue-Y. Huang](#), and [Jun J. Meng](#), A review of coarse mineral dust in the Earth system, [Aeolian Aeol.](#)
443 [Res. Arch.](#), 60, <https://doi.org/10.1016/j.aeolia.2022.100849>, 2023.

444
445 d’Almeida, G. A.: On the variability of desert aerosol radiative characteristics, *J. Geophys. Res. Atmos.*, 92, 3017–
446 3026, <https://doi.org/10.1029/JD092iD03p03017>, 1987.

447 d’Almeida, G. A. and Schütz, L.: Number, Mass and Volume Distributions of Mineral Aerosol and Soils of the Sahara,
448 *J. Climate Appl. Meteor.*, 22, 233–243, [https://doi.org/10.1175/1520-0450\(1983\)022<0233:NMAVDO>2.0.CO;2](https://doi.org/10.1175/1520-0450(1983)022<0233:NMAVDO>2.0.CO;2),
449 1983.

450 Bates, T. S., Coffman, D. J., Covert, D. S., and Quinn, P. K.: Regional marine boundary layer aerosol size distributions
451 in the Indian, Atlantic, and Pacific Oceans: A comparison of INDOEX measurements with ACE-1, ACE-2, and
452 Aerosols99, *J. Geophys. Res.*, 107, INX2 25–1–INX2 25–15, <https://doi.org/10.1029/2001JD001174>, 2002.

453 Baddock, M., Boskovic, L., Strong, C., McTainsh, G., Bullard, J., Agranovski, I., and Cropp, R.: Iron-rich nanoparticles
454 formed by aeolian abrasion of desert dune sand, *Geochemistry, Geophysics, Geosystems*, 14, 3720–3729,
455 <https://doi.org/10.1002/ggge.20229>, 2013.

456 Chen, G., Ziemba, L. D., Chu, D. A., Thornhill, K. L., Schuster, G. L., Winstead, E. L., Diskin, G. S., Ferrare, R. A.,
457 Burton, S. P., Ismail, S., Kooi, S. A., Omar, A. H., Slusher, D. L., Kleb, M. M., Reid, J. S., Twohy, C. H., Zhang, H., and
458 Anderson, B. E.: Observations of Saharan dust microphysical and optical properties from the Eastern Atlantic
459 during NAMMA airborne field campaign, *J. Geophys. Res.*, 11, 723–740, [https://doi.org/10.5194/acp-11-723-](https://doi.org/10.5194/acp-11-723-2011)
460 2011, 2011.

461 Chou, C., Formenti, P., Maille, M., Ausset, P., Helas, G., Harrison, M., and Osborne, S.: Size distribution, shape, and
462 composition of mineral dust aerosols collected during the African Monsoon Multidisciplinary Analysis Special
463 Observation Period 0: Dust and Biomass–Burning Experiment field campaign in Niger, *J. Geophys. Res.*, January
464 2006, 113, <https://doi.org/10.1029/2008JD009897>, 2008.

465 Claquin, T., Schulz, M., and Balkanski, Y.: Modeling the mineralogy of atmospheric dust sources, *J. Geophys. Res.*,
466 104, 22243–22256, 1999.

467 Clarke, A. D., Shinzuka, Y., Kapustin, V. N., Howell, S., Huebert, B., Doherty, S., Anderson, T., Covert, D., Anderson,
468 J., Hua, X., Moore, K. G., McNaughton, C., Carmichael, G., and Weber, R.: Size distributions and mixtures of dust
469 and black carbon aerosol in Asian outflow: Physiochemistry and optical properties, *J. Geophys. Res.*, 109,
470 <https://doi.org/10.1029/2003JD004378>, 2004.

471 Cuesta, J., Maxim Eremenko, C. Flamant, Gaëlle Dufour, Benoit Laurent, Gilles Bergametti, M. Hopfner, J. Orphal
472 and D. Zhou, Three-dimensional distribution of a major desert dust outbreak over East Asia in March 2008 derived
473 from IASI satellite observations, *J. Geophys. Res.*, 120, 7099–7127, 2015

474 Denjean, C., Formenti, P., Desboeufs, K., Chevaillier, S., Triquet, S., Maillé, M., Cazaunau, M., Laurent, B., Mayol-
475 Bracero, O. L., Vallejo, P., Quiñones, M., Gutierrez-Molina, I. E., Cassola, F., Prati, P., Andrews, E., and Ogren, J.:
476 Size distribution and optical properties of African mineral dust after intercontinental transport, *J. Geophys. Res.*,
477 121, 7117–7138, <https://doi.org/10.1002/2016JD024783>, 2016a.

478 Denjean, C., Cassola, F., Mazzino, A., Triquet, S., Chevaillier, S., Grand, N., Bourriane, T., Momboisse, G., Sellegri,
479 K., Schwarzenbock, A., Freney, E., Mallet, M., and Formenti, P.: Size distribution and optical properties of mineral
480 dust aerosols transported in the western Mediterranean, *Atmos. Chem. Phys.*, 16, 1081–1104,
481 <https://doi.org/10.5194/acp-16-1081-2016>, 2016b.

Mis en forme : Justifié, Retrait : Gauche : 0 cm

Mis en forme : Police : Non Italique

Mis en forme : Police : Non Italique

Mis en forme : Police : Non Italique

Code de champ modifié

Mis en forme : Police : 10 pt

Mis en forme : Police : (Par défaut) Times New Roman

Code de champ modifié

Code de champ modifié

Code de champ modifié

Code de champ modifié

Code de champ modifié

Mis en forme

482 [Di Biagio, C., Formenti, P., Balkanski, Y., Caponi, L., Cazaunau, M., Pangui, E., Journet, E., Nowak, S., Andreae, M.,](#)
483 [O., Kandler, K., Saeed, T., Piketh, S., Seibert, D., Williams, E., and Doussin, J.-F.: Complex refractive indices and](#)
484 [single-scattering albedo of global dust aerosols in the shortwave spectrum and relationship to size and iron](#)
485 [content, *Atmos. Chem. Phys.*, 19, 15503–15531, <https://doi.org/10.5194/acp-19-15503-2019>, 2019.](#)

486 Di Biagio, C., Y. Balkanski, S. Albani, O. Boucher, and P. Formenti, Direct radiative effect by mineral dust aerosols
487 constrained by new microphysical and spectral optical data, *Geophys. Res. Lett.*, 47, e2019GL086186.
488 <https://doi.org/10.1029/2019GL086186>, 2020.

489 Di Biagio, C., Doussin, J. F., Cazaunau, M., Pangui, E., Cuesta, J., Sellitto, P., Rodenas, M., and Formenti, P., Infrared
490 optical signature reveals the source-dependency and along-transport evolution of dust mineralogy as shown by
491 laboratory study, *Sci. Rep.*, 13, 13252, <https://doi.org/10.1038/s41598-023-39336-7>, 2023.

492 Dubovik, O., B. N. Holben, T. F. Eck, A. Smirnov, Y. J. Kaufman, M. D. King, D. Tanre, and I. Slutsker (2002), Variability
493 of absorption and optical properties of key aerosol types observed in worldwide locations, *J. Atmos. Sci.*, 59, 590–
494 608, doi:[10.1175/1520-0469\(2002\)059<0590:VOA](https://doi.org/10.1175/1520-0469(2002)059<0590:VOA).

495 Dubovik, O., et al. (2006), Application of spheroidal models to account for aerosol particle nonsphericity in remote
496 sensing of desert dust, *J. Geophys. Res.*, 111, D11208, doi:[10.1029/2005JD006619](https://doi.org/10.1029/2005JD006619).

497 Formenti, P., Andreae, M. O., Lange, L., Roberts, G., Cafmeyer, J., Rajta, I., Maenhaut, W., Holben, B. N., Artaxo, P.,
498 and Lelieveld, J.: Saharan dust in Brazil and Suriname during the Large-Scale Biosphere–Atmosphere Experiment
499 in Amazonia (LBA) – Cooperative LBA Regional Experiment (CLAIRE) in March 1998, *J. Geophys. Res.*, 106, 14919–
500 14934, <https://doi.org/10.1029/2000JD900827>, 2001.

501 Formenti, P., Rajot, J. L., Desboeufs, K., Saïd, F., Grand, N., Chevaillier, S., and Schmechtig, C.: Airborne observations
502 of mineral dust over western Africa in the summer Monsoon season: spatial and vertical variability of physico-
503 chemical and optical properties, *J. Geophys. Res.*, 11, 6387–6410, <https://doi.org/10.5194/acp-11-6387-2011>,
504 2011.

505 Formenti, P., Di Biagio, C., Huang, Y., Kok, J., Mallet, M. D., Boulanger, D., and Cazaunau, M.: Look-up tables
506 resolved by complex refractive index to correct particle sizes measured by common research-grade optical
507 particle counters, *Atmos. Meas. Tech. Discuss.* [preprint], <https://doi.org/10.5194/amt-2021-403>, in review,
508 2021.

509 Formenti P. and C Di Biagio, Large synthesis of in situ field measurements of the size distribution of mineral dust
510 aerosols across their lifecycle-SOURCE. <https://doi.org/10.57932/58dbe908-9394-4504-9099-74a3e77140e9>,
511 2023a.

512 Formenti P. and C Di Biagio, Large synthesis of in situ field measurements of the size distribution of mineral dust
513 aerosols across their lifecycle-MRT. <https://doi.org/10.57932/31f2adf7-74fb-48e8-a3ef-059f663c47f1>, 2023b.

514 Formenti P. and C Di Biagio, Large synthesis of in situ field measurements of the size distribution of mineral dust
515 aerosols across their lifecycle-LRT <https://doi.org/10.57932/17dc781c-3e9d-4908-85b5-5c99e68e8f79>, 2023c.

516 Fratini, G., Ciccioli, P., Febo, A., Forgione, A., and Valentini, R.: Size-segregated fluxes of mineral dust from a desert
517 area of northern China by eddy covariance, *Atmos. Chem. Phys.*, 7, 2839–2854, [https://doi.org/10.5194/acp-7-](https://doi.org/10.5194/acp-7-2839-2007)
518 [2839-2007](https://doi.org/10.5194/acp-7-2839-2007), 2007.

519 Gillette, D. A., Blifford, I. H., and Fenster, C. R.: Measurements of Aerosol Size Distributions and Vertical Fluxes of
520 Aerosols on Land Subject to Wind Erosion, *J. Appl. Meteor.*, 11, 977–987, [https://doi.org/10.1175/1520-](https://doi.org/10.1175/1520-0450(1972)011<0977:MOASDA>2.0.CO;2)
521 [0450\(1972\)011<0977:MOASDA>2.0.CO;2](https://doi.org/10.1175/1520-0450(1972)011<0977:MOASDA>2.0.CO;2), 1972.

522 Gillette, D.A. On the production of soil wind erosion having the potential for long range transport, *J. Rech. Atmos.*
523 8, 734–744, 1974.

524 Gillette, D. A., Blifford, I. H., and Fryrear, D. W.: The influence of wind velocity on the size distributions of aerosols
525 generated by the wind erosion of soils, *J. Geophys. Res.*, 79, 4068–4075,
526 <https://doi.org/10.1029/JC079i027p04068>, 1974.

527 Gomes, L., G. Bergametti, G. Coudé–Gaussen, and P. Rognon, Submicron Desert Dusts: A Sandblasting Process, *J.*
528 *Geophys. Res.*, 95 (D9), 927–940, 1990.

Mis en forme : Police :10 pt

Mis en forme : Justifié

Mis en forme : Police :Non Italique

Code de champ modifié

Mis en forme : Police :Non Italique

Code de champ modifié

Mis en forme : Police :Non Italique

Code de champ modifié

Mis en forme : Police :Non Italique

Code de champ modifié

Code de champ modifié

Code de champ modifié

Code de champ modifié

Mis en forme : Police :10 pt

Mis en forme : Non Surlignage

Mis en forme : Police :Non Italique

Mis en forme : Police : (Par défaut) + Titres (Calibri Light), 10 pt, Anglais (Royaume-Uni)

Mis en forme : Non Surlignage

Mis en forme

529 [Gómez Maqueo Anaya, S., Althausen, D., Faust, M., Baars, H., Heinold, B., Hofer, J., Tegen, I., Ansmann, A.,](#)
530 [Engelmann, R., Skupin, A., Heese, B., and Schepanski, K.: The implementation of dust mineralogy in COSMOS-05-](#)
531 [MUSCAT, *Geosci. Model Dev.*, 17, 1271–1295, <https://doi.org/10.5194/gmd-17-1271-2024>, 2024.](#)

532 [Gómez Maqueo Anaya, S., Althausen, D., Faust, M., Baars, H., Heinold, B., Hofer, J., Tegen, I., Ansmann, A.,](#)
533 [Engelmann, R., Skupin, A., Heese, B., and Schepanski, K.: The implementation of dust mineralogy in COSMOS-05-](#)
534 [MUSCAT, *EGUosphere* \[preprint\], <https://doi.org/10.5194/eguosphere-2023-1558>, 2023](#)

535 González-Flórez, C., Klose, M., Alastuey, A., Dupont, S., Escribano, J., Etyemezian, V., Gonzalez-Romero, A., Huang,
536 Y., Kandler, K., Nikolich, G., Panta, A., Querol, X., Reche, C., Yus-Díez, J., and Pérez García-Pando, C.: Insights into
537 the size-resolved dust emission from field measurements in the Moroccan Sahara, *Atmos. Chem. Phys.*, 23, 7177–
538 7212, <https://doi.org/10.5194/acp-23-7177-2023>, 2023.

539 Gonçalves Ageitos, M., V. Obiso, R.L. Miller, O. Jorba, M. Klose, M. Dawson, Y. Balkanski, J. Perlwitz, S. Basart, E. Di
540 Tomaso, J. Escribano, F. Macchia, G. Montané, N. Mahowald, R.O. Green, D.R. Thompson, and C. Pérez García-
541 Pando, 2023: Modeling dust mineralogical composition: sensitivity to soil mineralogy atlases and their expected
542 climate impacts, *Atmos. Chem. Phys.*, 23, no. 15, 8623–8657, doi:10.5194/acp-23-8623-2023.

543 [Green, R. O. et al. The earth surface mineral dust source investigation: an earth science imaging spectroscopy](#)
544 [mission. in: *2020 IEEE Aerospace Conference* 1–15 \(2020\). \[https://doi.org/10.1109/AERO47225.2020.91727\]\(https://doi.org/10.1109/AERO47225.2020.9172731\)](#)
545 [31.](#)

546 Huang, Y., Kok, J. F., Martin, R. L., Swet, N., Katra, I., Gill, T. E., Reynolds, R. L., and Freire, L. S.: Fine dust emissions
547 from active sands at coastal Oceano Dunes, California, 19, 2947–2964, [https://doi.org/10.5194/acp-19-2947-](https://doi.org/10.5194/acp-19-2947-2019)
548 [2019](#), 2019.

549 Huang, Y., Adebisi, A. A., Formenti, P., & Kok, J. F., Linking the different diameter types of aspherical desert dust
550 indicates that models underestimate coarse dust emission. *Geophys. Res. Lett.*, 48, e2020GL092054,
551 <https://doi.org/10.1029/2020GL092054>, 2021.

552 Huneus, N., Schulz, M., Balkanski, Y., Griesfeller, J., Prospero, J., Kinne, S., Bauer, S., Boucher, O., Chin, M.,
553 Dentener, F., Diehl, T., Easter, R., Fillmore, D., Ghan, S., Ginoux, P., Grini, A., Horowitz, L., Koch, D., Krol, M. C.,
554 Landing, W., Liu, X., Mahowald, N., Miller, R., Morcrette, J.-J., Myhre, G., Penner, J., Perlwitz, J., Stier, P., Takemura,
555 T., and Zender, C. S.: Global dust model intercomparison in AeroCom phase I, *Atmos. Chem. Phys.*, 11, 7781–7816,
556 <https://doi.org/10.5194/acp-11-7781-2011>.

557 Johnson, B. T. and Osborne, S. R.: Physical and optical properties of mineral dust aerosol measured by aircraft
558 during the GERBILS campaign, *Q. J. Royal. Met. Soc.*, 137, 1117–1130, <https://doi.org/10.1002/qj.777>, 2011.

559 Journet, E., Balkanski, Y., and Harrison, S. P.: A new data set of soil mineralogy for dust-cycle modeling, *Atmos.*
560 *Chem. Phys.*, 14, 3801–3816, <https://doi.org/10.5194/acp-14-3801-2014>, 2014.

561 Jung, E., Albrecht, B., Prospero, J. M., Jonsson, H. H., and Kreidenweis, S. M.: Vertical structure of aerosols,
562 temperature, and moisture associated with an intense African dust event observed over the eastern Caribbean,
563 *Journal of Geophysical Research: Atmospheres*, 118, 4623–4643, <https://doi.org/10.1002/jgrd.50352>,
564 2013.

565 Kaaden, N., Massling, A., Schladitz, A., Müller, T., Kandler, K., Schütz, L., Weinzierl, B., Petzold, A., Tesche, M.,
566 Leinert, S., Deutscher, C., Ebert, M., Weinbruch, S., and Wiedensohler, A.: State of mixing, shape factor, number
567 size distribution, and hygroscopic growth of the Saharan anthropogenic and mineral dust aerosol at Tinfou,
568 Morocco, *Tellus B*, 61, 51–63, <https://doi.org/10.1111/j.1600-0889.2008.00388.x>, 2009.

569 Kandler, K., Schütz, L., Deutscher, C., Ebert, M., Hofmann, H., JäCKEL, S., Jaenicke, R., Knippertz, P., Lieke, K.,
570 Massling, A., Petzold, A., Schladitz, A., Weinzierl, B., Wiedensohler, A., Zorn, S., and Weinbruch, S.: Size
571 distribution, mass concentration, chemical and mineralogical composition and derived optical parameters of the
572 boundary layer aerosol at Tinfou, Morocco, during SAMUM 2006, *Tellus B*, 61, 32–50,
573 <https://doi.org/10.1111/j.1600-0889.2008.00385.x>, 2009.

574 Kandler, K., Schütz, L., Jäckel, S., Lieke, K., Emmel, C., Müller-Ebert, D., Ebert, M., Scheuvs, D., Schladitz, A.,
575 Šegvić, B., Wiedensohler, A., and Weinbruch, S.: Ground-based off-line aerosol measurements at Praia, Cape
576 Verde, during the Saharan Mineral Dust Experiment: microphysical properties and mineralogy, *Tellus B*, 63, 459–
577 474, <https://doi.org/10.1111/j.1600-0889.2011.00546.x>, 2011.

Mis en forme : Police :10 pt

Code de champ modifié

Mis en forme : Français (France)

Code de champ modifié

Code de champ modifié

Mis en forme

- 578 Khalfallah, B., Bouet, C., Labiadh, M. T., Alfaro, S. C., Bergametti, G., Marticorena, B., Lafon, S., Chevaillier, S., Féron,
579 A., Hease, P., Tureaux, T. H. des, Sekrafi, S., Zapf, P., and Rajot, J. L.: Influence of Atmospheric Stability on the Size
580 Distribution of the Vertical Dust Flux Measured in Eroding Conditions Over a Flat Bare Sandy Field, *J. Geophys. Res.:*
581 *Atmos.*, 125, e2019JD031185, <https://doi.org/10.1029/2019JD031185>, 2020.
- 582 Knippertz, P. and Stuut, J.-B. W. (Eds.): Mineral Dust: A Key Player in the Earth System, Springer Netherlands,
583 <https://doi.org/10.1007/978-94-017-8978-3>, 2014.
- 584 Kobayashi, H., Arai, K., Murayama, T., Iokibe, K., Koga, R., and Shiobara, M.: High-Resolution Measurement of Size
585 Distributions of Asian Dust Using a Coulter Multisizer, *J. Atmos. Oceanic Technol.*, 24, 194–205,
586 <https://doi.org/10.1175/JTECH1965.1>, 2007.
- 587 Kok, J. F., ~~(2011)~~ A scaling theory for the size distribution of emitted dust aerosols suggests climate models
588 underestimate the size of the global dust cycle. *Proc Natl Acad Sci U S A* 108:1016–1021, 2011
- 589 Kok, J. F., Ridley, D. A., Zhou, Q., Miller, R. L., Zhao, C., Heald, C. L., Ward, D. S., Albani, S., and Haustein, K.: Smaller
590 desert dust cooling effect estimated from analysis of dust size and abundance, *Nat. Geo.* 10, 274–278,
591 <https://doi.org/10.1038/ngeo2912>, 2017.
- 592 Mahowald, N., Lindsay, K., Rothenberg, D., Doney, S. C., Moore, J. K., Thornton, P., Randerson, J. T., and Jones, C.
593 D.: Desert dust and anthropogenic aerosol interactions in the Community Climate System Model coupled-carbon-
594 climate model, *Biogeosciences*, 8, 387–414, <https://doi.org/10.5194/bg-8-387-2011>, 2011.
- 595 Maring, H., Savoie, D. L., Izaguirre, M. A., McCormick, C., Arimoto, R., Prospero, J. M., and Pilinis, C.: Aerosol
596 physical and optical properties and their relationship to aerosol composition in the free troposphere at Izaña,
597 Tenerife, Canary Islands, during July 1995, *J. Geophys. Res.*, 105, 14677–14700,
598 <https://doi.org/10.1029/2000JD900106>, 2000.
- 599 Maring, H., Savoie, D. L., Izaguirre, M. A., Custals, L., and Reid, J. S.: Mineral dust aerosol size distribution change
600 during atmospheric transport, *J. Geophys. Res.*, 108, <https://doi.org/10.1029/2002JD002536>, 2003.
- 601 McConnell, C. L., Highwood, E. J., Coe, H., Formenti, P., Anderson, B., Osborne, S., Nava, S., Desboeufs, K., Chen,
602 G., and Harrison, M. a. J.: Seasonal variations of the physical and optical characteristics of Saharan dust: Results
603 from the Dust Outflow and Deposition to the Ocean (DODO) experiment, *J. Geophys. Res.*, 113,
604 <https://doi.org/10.1029/2007JD009606>, 2008.
- 605 Meloni, D., Junkermann, W., Sarra, A. di, Cacciani, M., Silvestri, L. D., Iorio, T. D., Estellés, V., Gómez-Amo, J. L.,
606 Pace, G., and Sferlazzo, D. M.: Altitude-resolved shortwave and longwave radiative effects of desert dust in the
607 Mediterranean during the GAMARF campaign: Indications of a net daily cooling in the dust layer, *J. Geophys. Res.*,
608 120, 3386–3407, <https://doi.org/10.1002/2014JD022312>, 2015.
- 609 Meng, J., Huang, Y., Leung, D. M., Li, L., Adebisi, A. A., Ryder, C. L., Mahowald, N. M., and Kok, J. F.: Improved
610 Parameterization for the Size Distribution of Emitted Dust Aerosols Reduces Model Underestimation of Super
611 Coarse Dust, ~~Geophysical Research Letters~~, 49, e2021GL097287,
612 <https://doi.org/10.1029/2021GL097287>, 2022.
- 613 Menut, L., Siour, G., Bessagnet, B., Couvidat, F., Journet, E., Balkanski, Y., and Desboeufs, K.: Modelling the
614 mineralogical composition and solubility of mineral dust in the Mediterranean area with CHIMERE 2017r4, *Geosci.*
615 *Model Dev.*, 13, 2051–2071, <https://doi.org/10.5194/gmd-13-2051-2020>, 2020.
- 616 Müller, K., Lehmann, S., van Pinxteren, D., Gnauk, T., Niedermeier, N., Wiedensohler, A., and Herrmann, H.: Particle
617 characterization at the Cape Verde atmospheric observatory during the 2007 RHaMBLe intensive, 10, 2709–2721,
618 *Atmos. Chem. Phys.*, <https://doi.org/10.5194/acp-10-2709-2010>, 2010.
- 619 Osborne, S. R., Johnson, B. T., Haywood, J. M., Baran, A. J., Harrison, M. a. J., and McConnell, C. L.: Physical and
620 optical properties of mineral dust aerosol during the Dust and Biomass-burning Experiment, *J. Geophys. Res.*, 113,
621 <https://doi.org/10.1029/2007JD009551>, 2008.
- 622 Otto, S., de Reus, M., Trautmann, T., Thomas, A., Wendisch, M., and Borrmann, S.: Atmospheric radiative effects
623 of an in situ measured Saharan dust plume and the role of large particles, *Tellus B*, 7, 4887–4903,
624 <https://doi.org/10.5194/acp-7-4887-2007>, 2007.
- 625 Perlwitz, J.P., C. Pérez García-Pando, and R.L. Miller: Predicting the mineral composition of dust aerosols — Part
626 1: Representing key processes. *Atmos. Chem. Phys.*, 15, 11593–11627, [doi:10.5194/acp-15-11593-2015](https://doi.org/10.5194/acp-15-11593-2015), 2015a.

Code de champ modifié

Code de champ modifié

Mis en forme : Police : Non Italique

Mis en forme

627 Perlwitz, J.P., C. Pérez García-Pando, and R.L. Miller: Predicting the mineral composition of dust aerosols — Part
628 2: Model evaluation and identification of key processes with observations. *Atmos. Chem. Phys.*, **15**, 11629–11652,
629 doi:10.5194/acp-15-11629-2015, 2015b.

630 Rajot, J. L., Formenti, P., Alfaro, S., Desboeufs, K., Chevaillier, S., Chatenet, B., Gaudichet, A., Journet, E.,
631 Marticorena, B., Triquet, S., Maman, A., Mouget, N., and Zakou, A.: AMMA dust experiment: An overview of
632 measurements performed during the dry season special observation period (SOP0) at the Banizoumbou (Niger)
633 supersite, *J. Geophys. Res.*, **113**, <https://doi.org/10.1029/2008JD009906>, 2008.

634 Reid, E. A., Reid, J. S., Meier, M. M., Dunlap, M. R., Cliff, S. S., Broumas, A., Perry, K., and Maring, H.:
635 Characterization of African dust transported to Puerto Rico by individual particle and size segregated bulk analysis,
636 *J. Geophys. Res.*, **108**, <https://doi.org/10.1029/2002JD002935>, 2003a.

637 Reid, J. S., Jonsson, H. H., Maring, H. B., Smirnov, A., Savoie, D. L., Cliff, S. S., Reid, E. A., Livingston, J. M., Meier, M.
638 M., Dubovik, O., and Tsay, S.-C.: Comparison of size and morphological measurements of coarse mode dust
639 particles from Africa, *J. Geophys. Res.*, **108**, <https://doi.org/10.1029/2002JD002485>, 2003b.

640 Reid, J. S., Reid, E. A., Walker, A., Piketh, S., Cliff, S., Mandoos, A. A., Tsay, S.-C., and Eck, T. F.: Dynamics of
641 southwest Asian dust particle size characteristics with implications for global dust research, *J. Geophys. Res.*, **113**,
642 <https://doi.org/10.1029/2007JD009752>, 2008.

643 Renard, J.-B., Dulac, F., Durand, P., Bourgeois, Q., Denjean, C., Vignelles, D., Couté, B., Jeannot, M., Verdier, N.,
644 and Mallet, M.: In situ measurements of desert dust particles above the western Mediterranean Sea with the
645 balloon-borne Light Optical Aerosol Counter/sizer (LOAC) during the ChArMEx campaign of summer 2013, *Atmos.*
646 *Chem. Phys.*, **18**, 3677–3699, <https://doi.org/10.5194/acp-18-3677-2018>, 2018.

647 de Reus, M., Dentener, F., Thomas, A., Borrmann, S., Ström, J., and Lelieveld, J.: Airborne observations of dust
648 aerosol over the North Atlantic Ocean during ACE 2: Indications for heterogeneous ozone destruction, *J. Geophys.*
649 *Res.*, **105**, 15263–15275, <https://doi.org/10.1029/2000JD900164>, 2000.

650 Rosenberg, P. D., Dean, A. R., Williams, P. I., Dorsey, J. R., Minikin, A., Pickering, M. A., and Petzold, A.: Particle
651 sizing calibration with refractive index correction for light scattering optical particle counters and impacts upon
652 PCASP and CDP data collected during the Fennec campaign, *Atmos. Meas. Tech.*, **5**, 1147–1163,
653 <https://doi.org/10.5194/amt-5-1147-2012>, 2012.

654 Rosenberg, P. D., Parker, D. J., Ryder, C. L., Marsham, J. H., Garcia-Carreras, L., Dorsey, J. R., Brooks, I. M., Dean, A.
655 R., Crosier, J., McQuaid, J. B., and Washington, R.: Quantifying particle size and turbulent scale dependence of dust
656 flux in the Sahara using aircraft measurements, *J. Geophys. Res. Atmos.*, **119**, 7577–7598,
657 <https://doi.org/10.1002/2013JD021255>, 2014.

658 Ryder, C. L., Highwood, E. J., Lai, T. M., Sodemann, H., and Marsham, J. H.: Impact of atmospheric transport on the
659 evolution of microphysical and optical properties of Saharan dust, *Geophys. Res. Lett.*, **40**, 2433–2438,
660 <https://doi.org/10.1002/grl.50482>, 2013a.

661 Ryder, C. L., Highwood, E. J., Rosenberg, P. D., Trembath, J., Brooke, J. K., Bart, M., Dean, A., Crosier, J., Dorsey, J.,
662 Brindley, H., Banks, J., Marsham, J. H., McQuaid, J. B., Sodemann, H., and Washington, R.: Optical properties of
663 Saharan dust aerosol and contribution from the coarse mode as measured during the Fennec 2011 aircraft
664 campaign, *Atmos. Chem. Phys.*, **13**, 303–325, <https://doi.org/10.5194/acp-13-303-2013>, 2013b.

665 Ryder, C. L., Marengo, F., Brooke, J. K., Estelles, V., Cotton, R., Formenti, P., McQuaid, J. B., Price, H. C., Liu, D.,
666 Ausset, P., Rosenberg, P. D., Taylor, J. W., Choularton, T., Bower, K., Coe, H., Gallagher, M., Crosier, J., Lloyd, G.,
667 Highwood, E. J., and Murray, B. J.: Coarse-mode mineral dust size distributions, composition and optical properties
668 from AER-D aircraft measurements over the tropical eastern Atlantic, *Atmos. Chem. Phys.*, **18**, 17225–17257,
669 <https://doi.org/10.5194/acp-18-17225-2018>, 2018.

670 Scanza, R. A., Mahowald, N., Ghan, S., Zender, C. S., Kok, J. F., Liu, X., Zhang, Y., and Albani, S.: Modeling dust as
671 component minerals in the Community Atmosphere Model: development of framework and impact on radiative
672 forcing, *Atmos. Chem. Phys.*, **15**, 537–561, <https://doi.org/10.5194/acp-15-537-2015>, 2015.

673 Schladitz, A., Müller, T., Nowak, A., Kandler, K., Lieke, K., Massling, A., and Wiedensohler, A.: In situ aerosol
674 characterization at Cape Verde, *Tellus B.*, **63**, 531–548, <https://doi.org/10.1111/j.1600-0889.2011.00569.x>, 2011.

Mis en forme : Non souligné

Code de champ modifié

Mis en forme : Non souligné

Mis en forme : Police :Non Italique

Mis en forme : Police :Non Gras

Mis en forme : Police :10 pt, Non Italique

Mis en forme : Police :10 pt

Mis en forme : Police :10 pt, Non Italique

Mis en forme : Police :10 pt

Code de champ modifié

Mis en forme

675 Schütz, L. and Jaenicke, R.: Particle Number and Mass Distributions above 10–4 cm Radius in Sand and Aerosol of
676 the Sahara Desert, *J. Appl. Meteor.*, 13, 863–870, [https://doi.org/10.1175/1520-0450\(1974\)013<0863:PNAMDA>2.0.CO;2](https://doi.org/10.1175/1520-0450(1974)013<0863:PNAMDA>2.0.CO;2), 1974.

678 ~~Schütz, L., Jaenicke, R. and Pietrek, H.: Saharan Dust Transport over the North Atlantic Ocean. In: Péwé, T.L., Ed., Desert Dust, Geological Society of America, Boulder, Special Paper, Vol. 186, 87-100. <https://doi.org/10.1130/SPE186-p87>, 1981.~~

681 ~~Schütz, L., Jaenicke, R., and Pietrek, H.: Saharan dust transport over the North Atlantic Ocean, <https://doi.org/10.1130/SPE186-p87>, 1981.~~

683 Shao, Y., Ishizuka, M., Mikami, M., and Leys, J. F.: Parameterization of size-resolved dust emission and validation with measurements, *J. Geophys. Res.*, 116, <https://doi.org/10.1029/2010JD014527>, 2011.

685 Sow, M., Alfaro, S. C., Rajot, J. L., and Marticorena, B.: Size resolved dust emission fluxes measured in Niger during 3 dust storms of the AMMA experiment, *Atmos. Chem., Phys.*, 9, 3881–3891, <https://doi.org/10.5194/acp-9-3881-2009>, 2009.

688 Struckmeier, C., Drewnick, F., Fachinger, F., Gobbi, G. P., and Borrmann, S.: Atmospheric aerosols in Rome, Italy: sources, dynamics and spatial variations during two seasons, *Atmos. Chem. Phys.*, 16, 15277–15299, <https://doi.org/10.5194/acp-16-15277-2016>, 2016.

691 Sviridenkov, M. A., Gillette, D. A., Isakov, A. A., Sokolik, I. N., Smirnov, V. V., Belan, B. D., Pachenko, M. V., Andronova, A. V., Kolomiets, S. M., Zhukov, V. M., and Zhukovsky, D. A.: Size distributions of dust aerosol measured during the Soviet–American experiment in Tadzhikistan, 1989, *Atmospheric Atmos. Environment. Part Environ. A. General Topics*, 27, 2481–2486, [https://doi.org/10.1016/0960-1686\(93\)90019-U](https://doi.org/10.1016/0960-1686(93)90019-U), 1993.

695 Wagner, F., Bortoli, D., Pereira, S., Costa, M. Jo., Silva, A. M., Weinzierl, B., Esselborn, M., Petzold, A., Rasp, K., Heinold, B., and Tegen, I.: Properties of dust aerosol particles transported to Portugal from the Sahara desert, *Tellus B: Chemical and Physical Meteorology*, 61, 297–306, <https://doi.org/10.1111/j.1600-0889.2008.00393.x>, 2009.

699 Walsler, A., Sauer, D., Spanu, A., Gasteiger, J., and Weinzierl, B.: On the parametrization of optical particle counter response including instrument-induced broadening of size spectra and a self-consistent evaluation of calibration measurements, *Atmos. Chem. Phys.*, 10, 4341–4361, <https://doi.org/10.5194/amt-10-4341-2017>, 2017.

702 Weinzierl, B., Petzold, A., Esselborn, M., Wirth, M., Rasp, K., Kandler, K., Schütz, L., Koepke, P., and Fiebig, M.: Airborne measurements of dust layer properties, particle size distribution and mixing state of Saharan dust during SAMUM 2006, *Tellus B*, 61, 96–117, <https://doi.org/10.1111/j.1600-0889.2008.00392.x>, 2009.

705 Weinzierl, B., Sauer, D., Esselborn, M., Petzold, A., Veira, A., Rose, M., Mund, S., Wirth, M., Ansmann, A., Tesche, M., Gross, S., and Freudenthaler, V.: Microphysical and optical properties of dust and tropical biomass burning aerosol layers in the Cape Verde region—an overview of the airborne in situ and lidar measurements during SAMUM-2, *Tellus B*, 63, 589–618, <https://doi.org/10.1111/j.1600-0889.2011.00566.x>, 2011.

709 Weinzierl, B., Ansmann, A., Prospero, J. M., Althausen, D., Benker, N., Chouza, F., Dollner, M., Farrell, D., Fomba, W. K., Freudenthaler, V., Gasteiger, J., Groß, S., Haarig, M., Heinold, B., Kandler, K., Kristensen, T. B., Mayol-Bracero, O. L., Müller, T., Reitebuch, O., Sauer, D., Schäfler, A., Schepanski, K., Spanu, A., Tegen, I., Toledano, C., and Walsler, A.: The Saharan Aerosol Long-Range Transport and Aerosol–Cloud–Interaction Experiment: Overview and Selected Highlights, *Bull. Amer. Meteor. Soc.*, 98, 1427–1451, <https://doi.org/10.1175/BAMS-D-15-00142.1>, 2017.

715 Zhao, A., Ryder, C. L., and Wilcox, L. J.: How well do the CMIP6 models simulate dust aerosols?, *Atmos. Chem. Phys.*, 22, 2095–2119, <https://doi.org/10.5194/acp-22-2095-2022>, 2022.

717 Zhou, Y., R. C. Levy, et al. "Dust Aerosol Retrieval over the Oceans with the MODIS/VIIRS Dark Target algorithm. Part I: Dust Detection." *Earth and Space Science* n/a(n/a): e2020EA001221.

Mis en forme : Police :10 pt

Mis en forme : Police :10 pt

Mis en forme : Police :10 pt

Mis en forme : Police :10 pt, Non Italique

Mis en forme : Police :10 pt

Mis en forme : Police :10 pt

Mis en forme : Police :10 pt, Non Italique

Mis en forme : Police :10 pt

Mis en forme